Journal of Geophysical Research: Oceans

RESEARCH ARTICLE
10.1029/2018JC014365

Tidally Induced Overflow of the Faroese Channels Bottom Water Over the Wyville Thomson Ridge

Vasiliy Vlasenko[1] and **Nataliya Stashchuk**[1]

[1]School of Biological and Marine Sciences, University of Plymouth,Plymouth, UK

Key Points:
- Observational evidence of the Faroese Channels Bottom Water into the Darwin Mounds area is reported
- The observed overflow in the eastern part of the Wyville Thomson Ridge is replicated numerically
- Spring tidal currents across the Faroese Channels are responsible for the overflow

Correspondence to:
V. Vlasenko,
vvlasenko@plymouth.ac.uk

Citation:
Vlasenko, V., & Stashchuk, N. (2018). Tidally induced overflow of the Faroese channels bottom water over the Wyville Thomson Ridge. *Journal of Geophysical Research: Oceans*, *123*. https://doi.org/10.1029/2018JC014365

Received 13 JUL 2018
Accepted 4 SEP 2018
Accepted article online 7 SEP 2018

Abstract An overflow of dense cold water from the Faroese Channels across the Wyville Thomson Ridge (WTR) into the Rockall Trough was recorded during the 136th cruise of the RRS *James Cook* in June 2016. This event happened in the eastern part of the ridge. The remotely operated vehicle ISIS deployed for a collection of coral samples recorded an abrupt drop in temperature at 500-m depth. Specifically, the water temperature decreased from 8.73 to 6.74 °C and salinity from 35.26 to 35.16. This rapid drop happened over 20 min, with the fastest rate of water temperature decrease of 1.10 °C occurring just over 1 min 50 s. The numerical modeling conducted to reproduce the event has shown that a massive overflow took place in the WTR section, which is close to the Darwin Mounds. The overflow has led to resuspension of bottom sediments; the remotely operated vehicle sampling program in the area of the Darwin Mounds terminated due to low visibility. The numerical experiments have shown that tidally induced overflows over the WTR can occur periodically under spring tidal conditions. The model allowed us to identify two places in the eastern part of the WTR where the tidally driven overflows more realistically can happen.

Plain Language Summary The paper concerns deep water circulation in Northern Atlantic. A rare event of the Faroe-Shetland Bottom Waters overflow through the Wyville Thomson Ridge to the Darwin Mounds was registered during the 136th cruise of the Royal Research Ship *James Cook* in June 2016. The overflow was observed in the eastern segment of the Wyville Thomson Ridge. The reason for a spillage of the cold bottom waters from the Faroese Channels over the Wyville Thomson Ridge to the Darwin Mound is discussed in the paper based on the observational data and the results of numerical modeling. The Massachusetts Institute of Technology general circulation model reproduced the baroclinic tidal processes developed in the area. Numerical experiments confirmed a high probability of overflows induced by cross-channel tidal oscillations during spring tidal conditions.

1. Introduction

The water exchange across the Greenland-Iceland-Scotland Ridge is a part of the Atlantic Meridional Overturning Circulation. In this area warm, saline equatorial waters flow northward as surface currents, while cold fresher water returns back, partly in surface layers along the Greenland coast and partially as deep bottom currents overflowing the Greenland-Scotland Ridge in several locations (Hansen & Østerhus, 2000). The main part of southward moving Norwegian Sea Deep Water flows via Faroese Channels (FC), which include the Faroe-Shetland Channel (FSC), Wyville Thomson Basin, and the Faroe Bank Channel (FBC; Ellett, 1991; Kuijpers et al., 1998; Saunders, 1990; Figure 1a). The FBC overflow transports about 2.2 ± 0.2 Sv of FSC bottom waters (Hansen et al., 2016) feeding the Iceland-Scotland Overflow Water, which is one of the major deep water masses in the North Atlantic (Hansen & Østerhus, 2000).

The Wyville Thomson Ridge (WTR) separates the FSC and FBC from the southerly located Rockall Trough (RT), a steep-sided, deep water basin. This ridge, with its sill depth of 400–500 m, is a natural geological barrier that prevents penetration of the cold Faroe-Shetland Channel Bottom Water (FSCBW) from FSC to RT (see Figure 1a). As a result of a blockage, the deep cold water is normally constrained within the FSC and FBC flowing northwestward along the WTR to the FBC (yellow arrows in Figure 1a). A comprehensive analysis of the deep water dynamics in the area has been provided by McCurtney and Mauritzen (2001) who analyzed the historical conductivity, temperature and depth (CTD) station data and mooring time series recorded over last six decades and reconstructed a steady state circulation in the FCs.

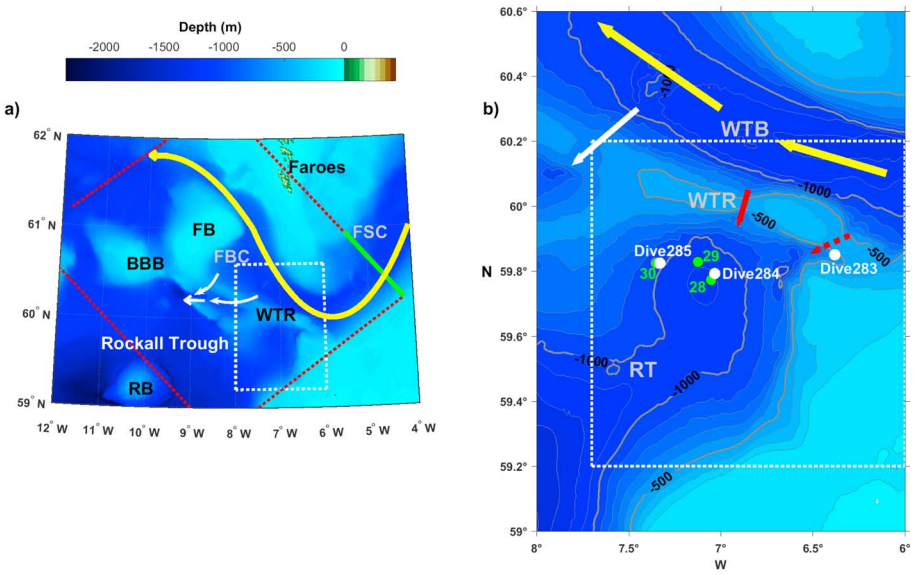

Figure 1. (a) Overview map showing main seabed topographic features of the Faroese Channels (FC), including Faroe-Shetland Channel (FSC), Wyville Thomson Ridge (WTR), and Faroe Bank Channel (FBC). Bathymetric features labeled: Faroe Bank (FB), Rosemary Bank (RB), and the Bill Bailey's Bank (BBB). Yellow arrow shows the main route of the bottom waters in the FC, and the white ones depict the most probable position of the WTR overflows. Red dotted lines show the boundaries of the model domain with the position of the lock shown by the green line. Zoom of the dashed rectangle is shown in panel (b). The red dotted arrow shows the position of the overflow event recorded during the JC136 cruise, and the solid red line depicts the location of the main overflow predicted by the model. The positions of the CTD stations and remotely operated vehicle dives are shown by green and white dots, respectively. The depth in both panels is shown in meters, and the contour interval between thick isobaths in panel (b) is 500 m. The topographic features include Wyville Thomson Basin (WTB) and the Rockall Trough (RT).

From time to time, the equilibrium conditions in the channels are violated, and the FSCBW escapes from the FBC in southeastward direction overflowing the WTR and penetrating into the RT (white arrows in Figure 1a). The FSCBW enters the RT through a deep and narrow channel that crosses the WTR crest at its deepest 644-m depth saddle point (Ellett & Roberts, 1973). As recently recognized (Johnson et al., 2010), the FSCBW overflowing the WTR makes a significant contribution to the formation of the intermediate water mass in the northern RT and the Hatton-Rockall Basin (Sherwin et al., 2015) located to the south and west of the WTR. One particularly strong WTR overflow was observed in situ and reported by Sherwin (2010). This overflow was recorded as a downslope propagated gravity current with maximum downstream velocity up to 1.2 m/s at a depth of about 100 m above the bottom.

In the present paper we analyze the observational data set that shows an alternative spill location for the WTR overflow. This event occurred in the eastern section of the WTR in June 2016 during the 136th cruise of the RRS *James Cook*. In this cruise, the observational campaign was focussed on the collection of biological species and video surveying in a wide area that included the WTR and RT. The principal tool for biological sampling in this cruise was the ROV ISIS 6500 (German et al., 2003) that collected cold water corals in the areas of the WTR, Rosemary Bank, George Bligh Bank, Rockall Bank, and Anton Dohrn Seamount.

The overflow that happened in the eastern section of the WTR (along red doted line, Figure 1b) resulted in a resuspension of bottom sediments that made all further ROV samplings in the RT area impossible. The analysis of this unusual overflow event and its driving forces is a principal goal of the present paper. Its structure is as follows. We start with the discussion of the data collected during the JC136 cruise. This section is followed by the model results that show some possible locations for the WTR overflow. The paper ends with the discussion and conclusions of the study.

2. Measurements

The measurements in the WTR area commenced with the deployment of the ROV for the collection of cold water coral samples. Figure 1b shows the position of the 283rd ROV dive on 4–5 June 2016 in the eastern part of the RT. During this dive, the ROV operated between 520- and 580-m depth. It was equipped with a Sea-Bird

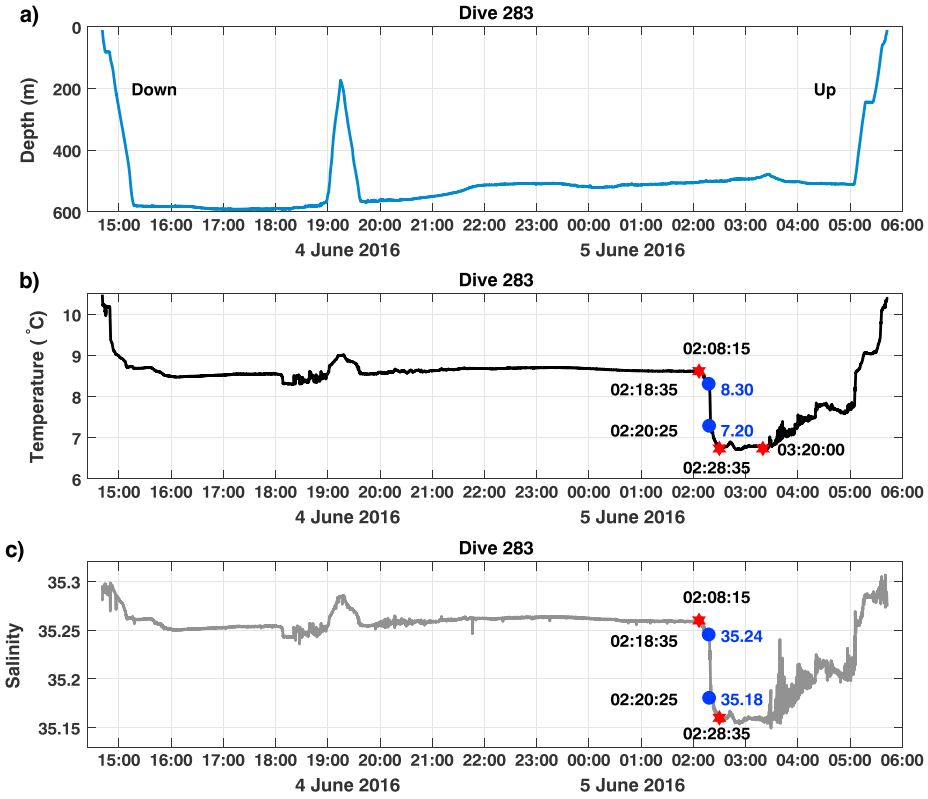

Figure 2. Time series of the 283rd ROV dive: (a) ROV's depth, (b) temperature, and (c) salinity recorded during the 283rd ROV dive. ROV = remotely operated vehicle.

SBE 49 CTD zond that measured standard oceanographic parameters during this mission. The time series in Figure 2a shows the descent of the ROV in the beginning and its ascent to the surface at the end of the dive. In between the ROV was flying 0.5 m above the bottom with mean velocity 0.05 m/s during 14 hr making some stops for the collection of samples. There was a minor technical issue at about 19:00 UTC on 4 June when the operators lost control on the ROV's position due to strong currents (more that 0.5 m/s), and it was urgently raised up to the 200-m depth. The ROV was returned to its mission 40 min later.

Figures 2b and 2c show the time series of temperature and salinity recorded during the dive. The most interesting fragment of the temperature and salinity time series (marked by red stars) is a sharp drop of temperature from 8.62 to 6.74°C and salinity from 35.26 to 35.16 over 20 min, which started at 02:08:15 UTC on 5 June. The fastest change of temperature and salinity was recorded at 02:18:35 UTC when the temperature dropped from 8.30 to 7.19°C and salinity from 35.24 to 35.18 in 1 min 50 s. During this time, the ROV experienced strong currents again, but the operators managed to stabilize it. Taking into account that the ROV was in a stationary position at this moment collecting samples, one can assume that an intrusion of different water masses was recorded.

The existence of another water type in the bottom layer is also evident from the comparison of the vertical profiles of temperature and salinity recorded in the beginning and at the end of the 283rd ROV mission, Figures 3a and 3b. Being mostly consistent above 450-m depth, both, the salinity and temperature profiles, are remarkably different below this level. The significant discrepancy in values suggests recording the other water mass near the bottom. This fact is confirmed by the comparison of the temperature and salinity (TS) diagrams presented in Figures 3c and 3d. Both curves show nearly similar profiles in the upper 450-m layer and appearance of denser water below this level at the end of the dive. In fact, water with the density higher than 27.37 kg/m^3 was not recorded at the beginning of the dive, Figure 3c. The straight line that connects the points with densities 27.37 and 27.47 kg/m^3 in Figure 3d can be treated as evidence of mixing of two water types.

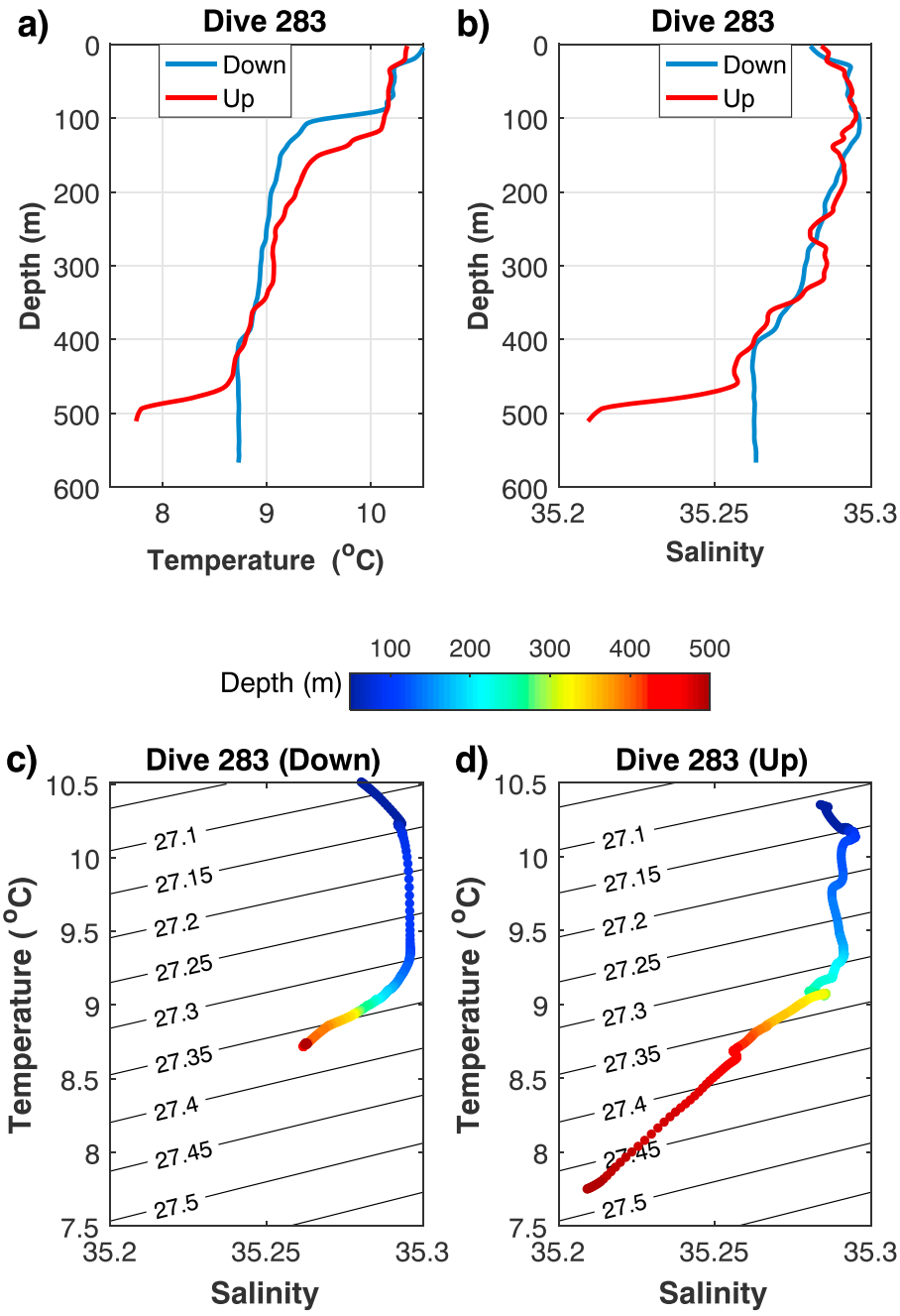

Figure 3. Temperature (a) and salinity (b) profiles recorded by the remotely operated vehicle during descent (blue) and ascent (red). TS diagrams for descent (c) and ascent (d) samplings. The color bars show the depth at the TS curves.

It was supposed that the most likely scenario of the processes developing during the 283rd ROV mission is a spillage of the FSCBW over the WTR in the eastern section of the ridge. Further observational evidence of this hypothesis was found in the middle of the hollow in the northward extent of the RT at the position of CTD stations 28–30, Figures 1b, where the Darwin Mounds are located (Masson et al., 2003). The latter form a cluster of individual mounds with their diameter up to 75 and 5 m high, which are associated with cold water corals *Lophelia pertusa*. In this area, the 284th dive of the ROV was carried out. Before the dive, the 28th CTD station was conducted, Figure 1b, with the aim to estimate visibility of near-bottom water whether it is transparent enough for ROV operation. The CTD sampling revealed a high level of turbidity in the bottom layer below 1,050-m depth. The turbidity readings here were 30 times larger than above this level, Figure 4a.

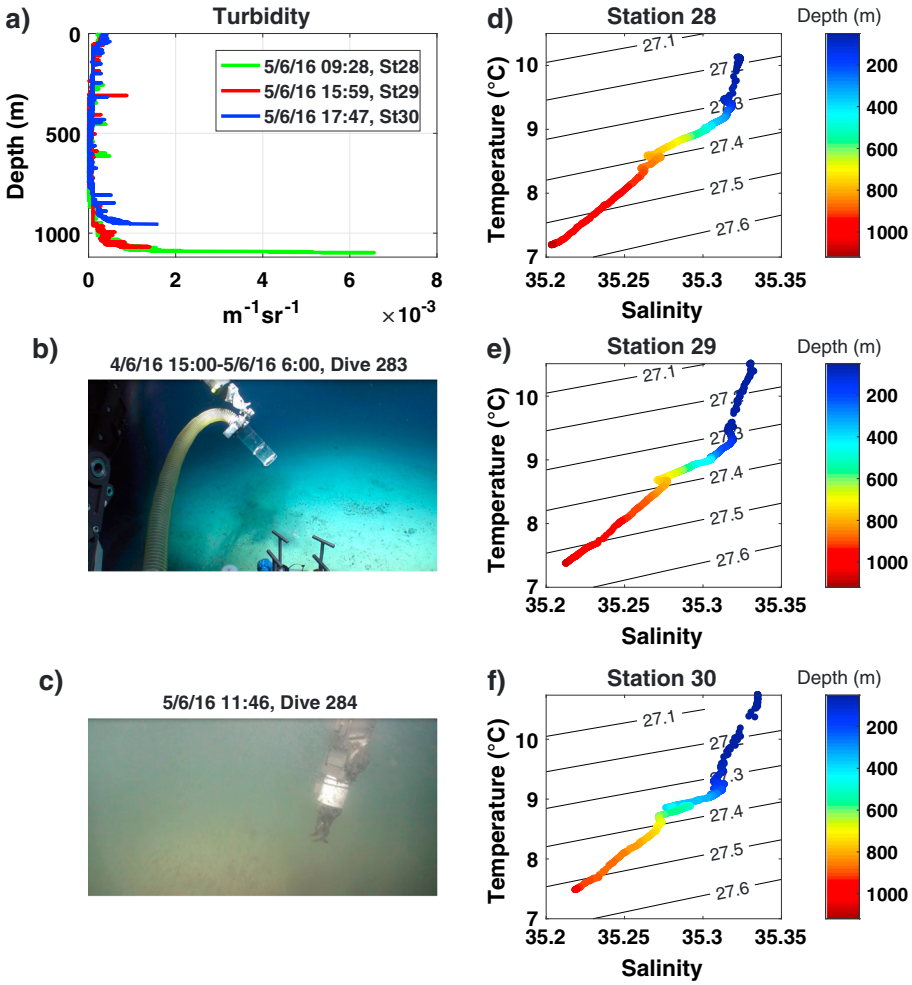

Figure 4. (a) Turbidity profiles recorded at CTD stations 28–30 on 5 June 2016. The unity for turbidity measurements in the operated SeaBird CTD zond was inverse meter times inverse steradian (sr; Sea-Bird Electronics, 2011). Images show visibility during (b) 283rd and (c) 284th remotely operated vehicle dives. TS diagrams for 28 (d), 29 (e), and 30 (f) CTD stations. The color bars show the depth in meters.

Note that a control CTD sampling in the area of the 283rd dive was not conducted, so the turbidity threshold for good visibility was unclear. In fact, it was hard to believe that good transparency of bottom waters at the position of the 283rd ROV's dive, Figure 4b, could be different in the area of the Darwin Mounds. Simple estimations based on the Stashchuk et al. (2010) modeling study show that in case the WTR overflow event in the area of the 283rd dive did take place, the downslope propagating gravity current could arrive at the 1,000-m isobath only 16 hr after the overflow started. The next 284th ROV mission was conducted 8 hr later after the end of the 283rd dive just in the center of the hollow at a point with coordinates 59.77°N, 7.05°W, and depth ~1,100 m (see Figure 1b). Note that visibility near the bottom in this place during the dive was very poor (less than 1 m, Figure 4c), so the ROV was immediately recovered after it reached the bottom. Seafloor sediments in the area of mounds contain predominantly quartz sand and sandy mud (Masson et al., 2003), which can be resuspended by bottom currents.

The 285th dive of the ROV conducted 9 hr later, and 17 km to the west of mission 284 (seemed to be distant from the assumed gravity current, see Figure 1b) was also unsuccessful due to poor visibility. Even though the level of turbidity in the bottom layer at CTD stations 29 and 30 conducted prior this dive was 3 times lower than that at station 28, the bottom water was still not transparent enough to proceed with samplings.

The reason for the sediments resuspension in the center of the hollow was not clear. The 284th sampling site was too far from the projected overflow site recorded during the 283rd dive. The presence of near-bottom intrusion of colder and fresher water at all three CTD stations was discovered from the analysis of the TS

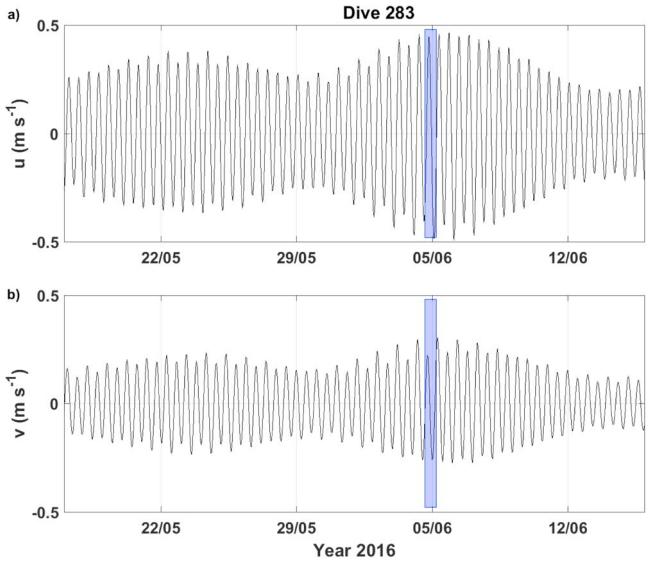

Figure 5. TPXO8.1 (European shelf model) predicted zonal (a) and meridional (b) tidal velocities in the area of the 283rd remotely operated vehicle dive. The blue boxes show the time of the dive.

diagrams shown in Figures 4d–4f. The shape of all TS diagrams resembles the curve shown in Figure 3d. The straight lines below 800-m depth in all three diagrams are typical for mixing of two water masses (Mamaev, 2010).

Another important conclusion that can be drawn from Figures 2b and 2c is the temperature and salinity time series recorded during 283rd ROV dive on 5 June were reversible. Specifically, after the intrusion event has been detected at 02:18:35 UTC, relatively stable temperature and salinity readings were recorded just over only 50 min (from 02:28:35 to 03:19:45 UTC, see Figures 2b and 2c). After this stabilizing period, these two parameters started recovering their initial values. Note that during this period the ROV was in a relatively stable position operating along 506-m isobath, Figures 2a (the ROV shifted only 1.35 km eastward during its 14-hr dive moving from the point with coordinates 59°50.752′N, 6°23.766′W to 59°51.235′N, 6°22.696′W). This stationary position of the ROV assumes that the increase of salinity and temperature in the bottom layer was a consequence of some local dynamical processes developing in the area, presumably an oscillating character of the recorded intrusion. In light of this fact it looks unlikely that the FSCBW overflow recorded in the area of the 283rd ROV dive at the flank of the WTR could reach the center of the RT hollow, that is, the place of the 284th and 285th ROV's dives. At the same time, poor visibility during these two dives (Figure 4c) and TS diagrams in positions of 28–30 CTD stations (Figures 4d–4f) evidences the development of some oceanographic processes that were not caught by observations.

Summarizing the observational data set collected in the RT on 4–5 June 2016, one can presume that the overflow event occasionally recorded at the northeastern flank of the WTR during the 283rd ROV dive was not a local phenomenon but had a more significant regional effect. Clarification of the reasons for the observed overflow is the primary target of the rest of this paper.

3. Modeling

A series of model experiments were conducted for the FBC area (for instance, Broadbridge & Toumi, 2015; Riemenschneider & Legg, 2007). The primary target of these numerical investigations was a reproduction of the deep water circulation in the FCs. Replication of the WTR overflow was not in the focus of these studies because of a relatively coarse grid for which the water spillage over the WTR was mostly a subgrid phenomenon. The detailed structure and the conditions at which the WTR overflow is formed were studied in the course of a fine-resolution modeling by Stashchuk et al. (2011) and Cuthbertson et al. (2014). They found that the most likely place for the WTR overflow is a saddle point located on its western side between the central gap and the Faroe Bank (see white arrow in Figure 1b) where most of the observational data on the WTR overflows have been collected (Sherwin, 2010; Sherwin et al., 2008; Sherwin & Turrell, 2005). A summary of these fine-resolution numerical experiments is presented below in section 3.1.

Note that all previous numerical studies on water circulation in the FCs did not include tidal forcing into the models. It was assumed that such short-term processes as tides could not contribute to the formation of large-scale bottom water circulation in the FC. It is worth mentioning here that Sherwin (1991) reported the observational evidence of large internal tidal waves in the area. This finding motivated modeling experiments conducted by Gerkema (2002) and Hall et al. (2011) who investigated the tidally generated internal waves, although without analysis of the deep water circulation in the FCs.

In this paper, we present a new series of numerical experiments that includes the formation of the deep water circulation in the FCs due to buoyancy fluxes and the spring tidal activity, Figure 5, that can initiate the overflow events. The Massachusetts Institute of Technology general circulation model (Marshall et al., 1997) is used as a modeling tool. The model domain is presented in Figure 1a by the red dotted rectangle. It includes the FSC, the WTR, and the northern part of the RT. The model grid was 568 × 628 with 500-m horizontal resolution. In the vertical direction the grid resolution was 5 m in the layer between 300 and 580 m and 10 m in the surface and bottom layers.

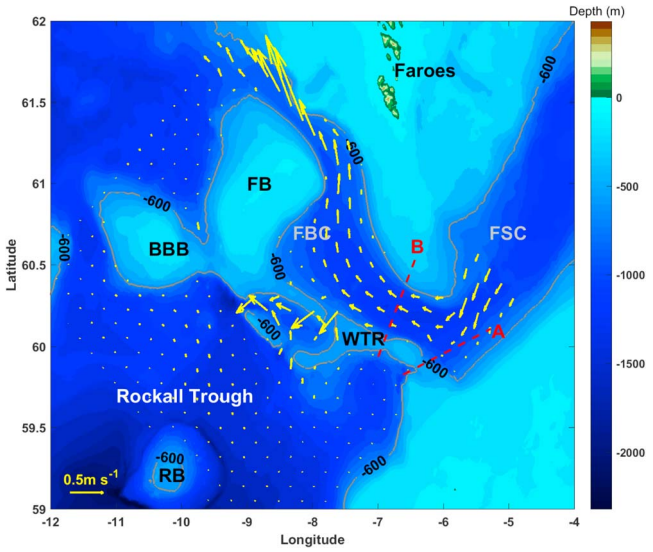

Figure 6. Horizontal circulation at 600-m depth after 60 days of the model time. Arrows give the magnitude and direction of the currents. Red lines show the transects A and B. FB = Faroe Bank; BBB = Bill Bailey's Bank; FSC = Faroe-Shetland Channel; WTR = Wyville Thomson Ridge; RB = Rosemary Bank; FBC = Faroe Bank Channel.

A two-step methodology of the numerical experiments was applied. The deep water circulation in the basin was established first in the course of a 60-day lock exchange experiment, and after that the tidal forcing was activated. Such an approach allows to eliminate from the analysis all transitional processes initiated at the beginning of the lock exchange experiment and to quantify the tidal contribution to the FBC circulation more accurately. The details of the model experiments were as follows.

3.1. Formation of the Deep Water Circulation in the FCs

The initial domain-wide distributions of temperature and salinity were taken from the measurements conducted in the RT (Stashchuk et al., 2010). The position of the lock was below 600-m depth at the northeastern boundary of the model domain (the green segment in Figure 1a). It separated the Norwegian Sea Water Masses that have the temperature <0° and salinity 34.9. When the lock was released, the cold water entered the area with velocity 0.15 m/s. Stashchuk et al. (2011) present all details of this lock exchange experiment.

The horizontal viscosity in the model was set according to Leith (1996), the scheme in which the viscosity is proportional to the horizontal gradient of relative vorticity and the cubed grid spacing. The Richardson number-dependent parametrization was used for setting vertical viscosity ν and diffusivity κ (Pacanowski & Philander, 1981):

$$\nu = \frac{\nu_0}{(1+\alpha Ri)^n} + \nu_b, \qquad \kappa = \frac{\nu}{(1+\alpha Ri)} + \kappa_b. \tag{1}$$

Here Ri is the Richardson number, $Ri = N^2(z)/(u_z^2 + v_z^2)$, and $N^2(z) = -g/\rho(\partial\rho/\partial z)$ is the buoyancy frequency (g is the acceleration due to gravity, and ρ is the density), u and v are the components of horizontal velocity; ν_b=10^{-5} m^2/s and κ_b=10^{-5} m^2/s are the background parameters, ν_0=1.5·10^{-2} m^2/s, α=5 and n=1 are the adjustable parameters.

It was found that the deep water circulation in a rotating channel (with mean latitude 61.5°N) was unstable in the beginning after the lock was released. Several local cyclonic and anticyclonic eddies were generated and dissipated at the first stage of the experiment (Stashchuk et al., 2011). The lifetime of these local cyclonic eddies was short (did not exceed ten days). The channel scale anticyclonic eddy that was formed upstream the crest of the FBC lived much longer, about 50 days.

A steady state circulation established in the channels after 60 days is shown in Figure 6 (the steady state is achieved when the water transport along the FBC does not change). It shows a relatively moderate current in the most of the model domain with their intensification in a narrow exit from the FBC. The cross-WTR currents are also clearly seen.

In vertical direction and across the channel the established thermohaline structure was characterized by pinching of the isotherms (isopycnals) at the southern flank of the WTR, which resulted in the concentration of cold water on the southern side of the FCs, Figure 7a. At the entrance to the FBC (transect A in Figure 6), the interface between the cold bottom FSCBW and the overlaying warmer waters is nearly horizontal, Figure 7b.

3.2. Tidal Forcing

After the establishment of the deep water circulation in the FC basin, the tidal forcing was activated in the model by setting a tidal potential in the right-hand side of the momentum balance equations. The intensity of the tidal forcing coincided with the predictions of the inverse tidal model TPXO8.1 (Egbert & Erofeeva, 2002). Figure 5 shows the TPXO model output for the cruise time. Specifically, the time of the 283rd ROV dive is depicted here by the blue rectangles. As it is clear from the tidal velocities time series, the ROV operated in the WTR area during the spring tidal phase when the tidal activity was maximal. The spatial distribution of the tidal forcing in the model domain is presented in Figure 8 as a system of tidal ellipses.

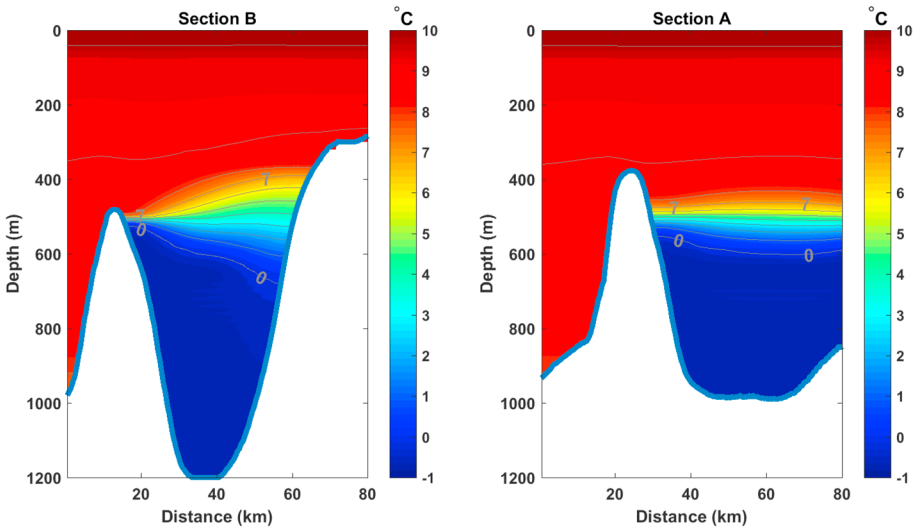

Figure 7. Temperature distributions along transects A and B, same as Figure 6.

The most probable reason for the observed WTR overflow was the spring tidal activity at the time of the 283rd ROV's dive. To check this hypothesis, the model with active tidal forcing was run additional 120 hr after the establishment of a steady state circulation in the FCs.

The across-ridge tidal oscillations resulted in an ultimate spillage of the FSCBW over the WTR, Figure 9 (note that we focus here on the JC136 field campaign area leaving apart the main overflow route depicted in Figure 6 and discussed in Cuthbertson et al., 2014; Stashchuk et al., 2011). Figure 9a presents the bottom water temperature after four tidal cycles. It reveals two places where the WTR overflow took place: (i) an intrusion of cold bottom water at the position of the 283rd ROV dive, Figure 1; and (ii) the spillage of cold water down to the Darwin Mounds at the location of CTD stations 28–30 where a high level of turbidity near the bottom was recorded, Figures 4a and 4c. It worth mentioning here that the overflowed water is a bit warmer than the FSCBW due to the mixing with overlying waters, Figure 7.

An additional transport equation for a passive tracer was added to the governing system to visualize the cold water overflow. The tracer concentration was set 1 in the bottom layer where the water temperature was below 7 °C and 0 in the rest of the model domain.

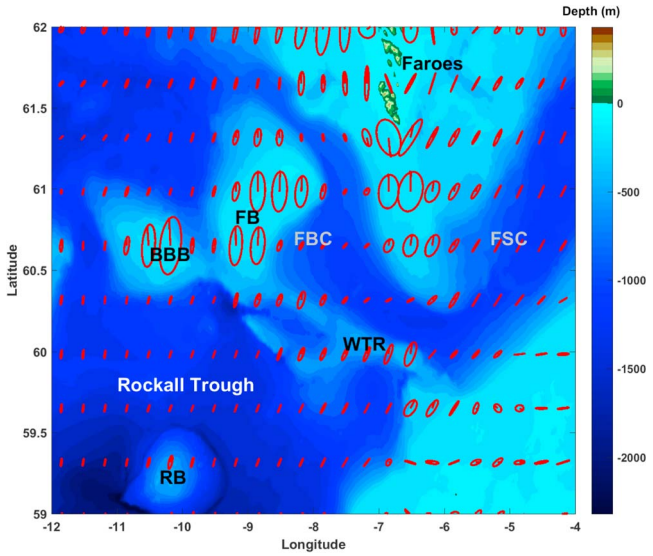

Figure 8. TPXO8.1 predicted tidal ellipses activated in the model as an external forcing. FB = Faroe Bank; BBB = Bill Bailey's Bank; FBC = Faroe Bank Channel; FSC = Faroe-Shetland Channel; WTR = Wyville Thomson Ridge; RB = Rosemary Bank.

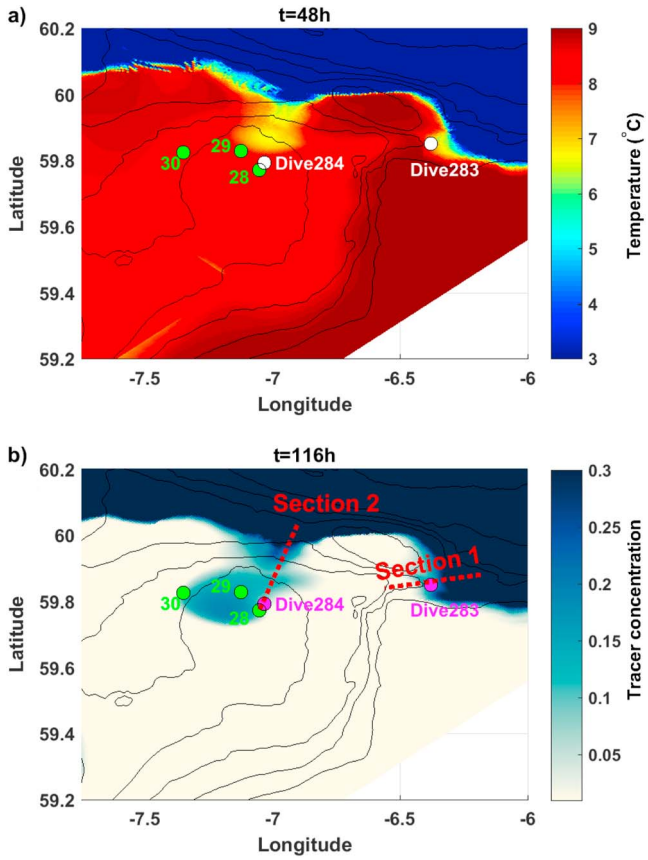

Figure 9. (a) The bottom temperature in the Rockall Trough area after four periods of tidal forcing. The model domain is shown in Figure 1a by the dashed rectangular. (b) Distribution of the passive tracer at the bottom after 10 tidal cycles.

The passive tracer field shown in Figure 9b demonstrates the positions and spatial scale of the overflow more clearly. Two major routes of the intrusion of the FSCBW into the RT are marked by sections 1 and 2. It is clear from the model runs that massive cold water overflows to the RT took place in the area of section 2 but not in section 1 where the ROV operated during its 283rd dive. The analysis of the model output has shown that the overflow happened during the tidal phase when the tidal current was directed southwestward across the WTR.

Being advected to the southern flank of the ridge, the FSCBW behaves differently in sections 1 and 2. In the area of the 283rd ROV's dive the intruded cold water does not propagate much beyond the ridge summit. Its maximum penetration length is shown in Figure 10a. The intrusion covers the area of the ROV's dive, but the FSCBW is advected back to the ridge top during the ebbing tidal phase; see Figure 10b.

The observational evidence of a similar water retreat is clearly seen in Figures 2b and 2c. After a sharp drop of the temperature and salinity recorded between 02:08 and 02:29 UTC, both parameter started recovering their initial values when the ebbing tidal flow advected the FSCBW back to the WTR summit. The tidal activity is probably the only reasonable explanation of the temporal variability shown in Figures 2b and 2c.

Summarizing the model results, one can conclude that there was no massive overflow event along section 1. It was just a small-scale cold water intrusion that ultimately mixed with surrounding waters and returned to the WTR summit. The model predicts quite a different scenario for the tidally induced water propagation in the area of section 2; see Figure 9b. Here the WTR overflow can have a form of a gravity current moving downslope from the ridge top. Figure 11 shows the boundary of this gravity current at different moments of time. This figure illustrates that the gravity current can reach the position of CTD station 28 three days after the beginning of the cold water spillage.

It is worth mentioning here that tidal periodicity of the overflow phenomenon assumes that the water outflow in section 2 does not take place permanently. It occurs periodically when the cross-ridge tidal current is

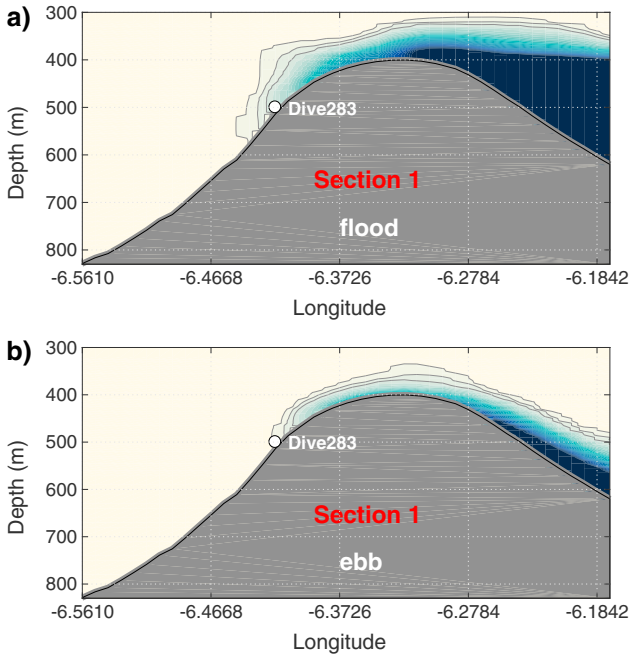

Figure 10. Position of the passive tracer along transect 1 (shown in Figure 9b) at flooding (a) and ebbing (b) tidal phases (114 hr [a] and 120 hr [b] after the tidal forcing was activated). The outer contour of the tracer intrusion is 0.01 with 0.01 contour interval.

strong enough to initiate the overflow. It is unclear yet what are the necessary and sufficient conditions for the initiation of the tidally induced overflow in the eastern part of the WTR.

The results presented in Figures 9–11 were obtained for the conditions of the highest spring tides that were observed during the JC136 cruise to the WTR, Figures 5a and 5b. A series of sensitivity runs were conducted for weaker tidal forcing that is typical for the neap tidal conditions or transition phase from the neap to spring tide. These runs have shown that 30% weaker tidal forcing than that depicted in blue boxes in Figures 5a and 5b (the highest spring tide in the area) does not initiate any substantial WTR overflow. With this forcing the cold FSCBW can penetrate into the southern flank of the WTR, but it does not propagate deep enough to reach the 800-m isobath.

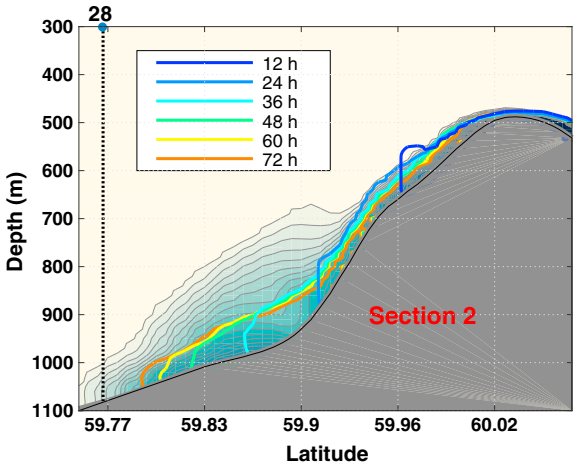

Figure 11. Evolution of the passive tracer along transect 2 during the overflow. Thick lines show the position of the outer boundary of the gravity current with concentration 0.1 at different moments of time (see the legend for the time). Thin lines depict the passive tracer plume after 10 tidal cycles. The concentration of the outer isoline equals 0.01 with 0.01 increment toward the plume core. The position of station 28 is shown by dotted line.

4. Discussion and Conclusions

The WTR separates the RT from the FSC and blocks the deep water overflow toward the RT. The upper boundary of the cold Norwegian Sea Deep Water flowing along the FBC is at the level of the WTR crest. Thus, in normal steady state conditions, the FSCBW is unable to overflow the WTR. However, under nonstationary conditions the most probable place for the WTR overflow is the saddle point located on its western side between the central gap and the Faroe Bank (see white arrows in Figure 1; Ellett, 1998; Ellett & Roberts, 1973; Sherwin et al., 2008; Sherwin & Turrell, 2005).

The detailed analysis of the water circulation in the area was conducted by McCurtney and Mauritzen (2001) who tested *the deep source* and *the shallow source* hypothesis on the water transport based on the observational data collected in the WTR area over last six decades (CTD stations and mooring data). The data collected by near-bottom instruments suggest that the Ridge blocks cold water inflow from the FCs to the RT in the eastern part of the WTR, and the spillover across it occurs farther west. Note, however, that some fragments of the unfiltered mooring recorded current time series clearly show that cold water intrusions into the RT can sporadically also occur in the eastern part of the WTR; see Figure 16c in McCurtney and Mauritzen (2001), although the authors did not clarify the reason for the recorded overflows.

In this paper we report observational evidence of cold bottom water overflow that happened in the eastern part of the WTR (find the red arrow in Figure 1b). The time of the overflow event coincided with the strongest spring tide, Figures 5a and 5b. The most probable reason for the water spillage over the WTR was a coincidence of several favorable factors such as intensification of the bottom water circulation in the FSC (reported by Sherwin et al., 2008) and strong spring tidal activity that occurred during the JC136 cruise.

The hypothesis on the possible tidal origin of the WTR overflow was in the focus of the present study. Numerical modeling complemented the collected observational data set. The Massachusetts Institute of Technology general circulation model was configured in such a way to replicate the dynamical processes developing in the FCs. The model settings were similar to that reported in Stashchuk et al. (2011). Several numerical experiments were conducted to quantify the tidal effect. Tidal forcing was changed from neap to spring conditions. The modeling study has shown that the *overflow event* recorded by the ROV during its 283rd dive was not an actual overflow. The FSCBW did cross the top of the WTR in the area of the 283rd ROV dive with the east-west flooding tidal flow (see Figure 10a). However, most of this water returned to the FBC with the ebbing tidal flow, see Figure 10b. Figures 2b and 2c show that the temperature and salinity started a slow recovery to their initial values after 1 hr of a sudden drop.

The principal finding from this study is that we identified the place where the tidally driven WTR overflows can occur. It is located 1° to the west from the 283rd ROV dive, Figure 9b. In this area, the oscillating across the WTR tidal flow entrains the FSCBW allowing its spillage over the WTR with downslope propagation as a gravity current (Figure 11).

As an indirect confirmation of this mechanism, a high level of near-bottom water turbidity was recorded just in the center of the hollow during the 284th and 285th ROV dives, Figure 1b. The images shown in Figure 4c with low visibility near the bottom and high level of turbidity depicted in Figure 4a can be explained by a sudden WTR overflow that happened due to tidal spring conditions.

Numerical experiments have shown that it is highly unlikely that the WTR overflow can happen during the neap tidal phase. With typical conditions taken for the incoming from the FC buoyancy fluxes and a standard FBC circulation, the tidal oscillations can initiate overflows during the spring tidal phase.

In the reported here numerical experiments the FSCBW enters the model domain with an initial horizontal velocity of 0.15 m/s (about 2.5 $\times 10^6$ m^3/s, or 2.5 Sv), which was chosen on the basis of an analysis of the acoustic Doppler current profiler data reported by Turrell and Sherwin (2003) and Sherwin et al. (2008). Some extra runs were conducted with different values of horizontal velocity: 0.2, 0.1, and 0.05 m/s as well as a deeper level (700 m) of FSCBW to investigate the sensitivity of the model results to the strength and depth of the inflow. It was found that with weaker discharge the FSCBW overflow to the Darwin Mounds does not happen even at spring tidal conditions.

It worth mentioning that the overflow recorded in the eastern part of the WTR hardly contributes substantially to the formation of intermediate water mass in the northern RT and the Hatton-Rockall Basin. The calculations of the water transport predicted by the model show that in the best-case scenario, that is, under spring tidal

conditions, the maximum discharge of the cold bottom water across the WTR in its eastern part can reach 0.3 Sv, which is substantially less than 2.2 ± 0.2 Sv calculated for the FBC overflow (Hansen et al., 2016) and 2 times weaker than that estimated for the western saddle point of the WTR (Stashchuk et al., 2011). Outside the spring tidal phases, the cold FCs bottom water is blocked by the WTR from its overflow to the RT.

Minor contribution of the overflows in the eastern part of the WTR to the formation of global oceanic circulation does not mean that they can be ignored in a broader context. The biological response of these overflows is likely to be significant. The WTR represents a physical barrier to the southward flowing cold Arctic waters. Faunal communities north and south of the ridge below the summit depth of approximately 500 m are highly distinct (Bett, 2001).

It is possible that the nutrient composition of the overflow water provides favorable (and unfavorable) conditions for a range of different species and thus alters community structure both by physical and biological mechanisms along the path of the overflow. The overflowing waters may also provide a mechanism by which the larvae can move into the RT. Biological sampling, community, and molecular analysis would be required to test these hypotheses. The potential for larvae to be transported into the RT from the FSC via overflowing water is crucial to determining biogeographic patterns in the deep sea. Thus, observations confirming overflow in this region will enable a better understanding of faunal biogeography than was previously possible.

Another exciting feature of the JC136 studied area is a cluster of the Darwin Mounds discovered during the RRS *Charles Darwin* cruise in 1989 (Bett, 2001). They are small cold water coral mounds, each 5 m high and up to 75 m across, located at a depth about 1,000 m. These mounds are the home for many species including *Lophelia pertusa*, which usually grow only on rocky surface, but here it feels quite comfortable in sandy conditions (Huvenne et al., 2016), presumably because of periodical overflows of the FSCBW through the WTR.

Geographically wise, the Darwin Mounds were classified according to their location, the Western (950-m depth) and the Eastern (1,000-m depth) Mounds. The position of CTD station 30 was right in the middle of the Western Mounds, and station 28 was to the south of the Eastern Mounds. In general, it is entirely possible that the overflows as that recorded in the JC136 cruise could provide favorable conditions for species living in the area of the Darwin Mounds through strong nutrient pathways, although this hypothesis still needs to be verified.

Acknowledgments
This work was supported by the UK NERC grant NE/K011855/1. The authors would like to thank the Captains, Crews, and Scientific Parties of all the cruises, especially the ROV ISIS team working during the JC136 cruise. We thank Bill Turrell and the anonymous reviewers for their valuable advises. The used data are available at https://figshare.com/articles/Untitled_Item/6169250. More details on the 136th Cruise of the RRS *James Cook* can be found at https://deeplinksproject.wordpress.com/ and https://www.bodc.ac.uk/resources/inventories/cruise_inventory/report/16050/.

References

Bett, B. J. (2001). UK Atlantic margin environmental survey: Introduction and overview of bathyal benthic ecology. *Continental Shelf Research*, *21*(8), 917–956.

Broadbridge, M. B., & Toumi, R. (2015). The deep circulation of the Faroe-Shetland Channel: Opposing flows and topographic eddies. *Journal of Geophysical Research: Oceans*, *120*, 5983–5996. https://doi.org/10.1002/2015JC010833

Cuthbertson, A., Davies, P. A., Stashchuk, N., & Vlasenko, V. (2014). Model studies of dense water overflows in the Faroese Channels. *Ocean Dynamics*, *64*, 273–292. https://doi.org/10.1007/s10236-013-0685-2

Egbert, G. D., & Erofeeva, S. Y. (2002). Efficient inverse modeling of barotropic ocean tides. *Journal of Atmospheric and Oceanic Technology*, *19*(2), 183–204.

Ellett, D. J. (1991). Norwegian Sea Deep Water overflow across the Wyville-Thomson Ridge during 1987–88. International Council for the Exploration of the Sea (ICES) CM1991/C:41.

Ellett, D. J. (1998). Norwegian Sea Deep Water overflow across the Wyville Thomson Ridge during 1987–88. *ICES Cooperative Research Report*, *225*, 195–205.

Ellett, D. J., & Roberts, D. G. (1973). The overflow of Norwegian Sea Deep Water across the Wyville-Thomson Ridge. *Deep Sea Research*, *20*, 819–835.

Gerkema, T. (2002). Application of an internal tidal generation model to baroclinic spring-neap cycles. *Journal of Geophysical Research*, *107*(C9), 3124. https://doi.org/10.1029/2001JC001177

German, C., Tyler, P., & Griffiths, G. (2003). The maiden voyage of UK ROV "Isis". *Ocean Challenge*, *12*(3), 16–18.

Hall, R. A., Huthnance, J. M., & Williams, R. G. (2011). Internal tides, nonlinear internal wave trains, and mixing in the Faroe-Shetland Channel. *Journal of Geophysical Research*, *116*, C03008. https://doi.org/10.1029/2010JC006213

Hansen, B., Larsen, K. M., Hátún, H., & Østerhus, S. (2016). A stable Faroe Bank Channel overflow 1995–2015. *Ocean Science*, *12*, 1205–1220.

Hansen, B., & Østerhus, S. (2000). North Atlantic-Nordic seas exchanges. *Progress in Oceanography*, *45*, 109–208.

Huvenne, V. A. I., Bett, B. J., Masson, D. G., Le Bas, T. P., & Wheeler, A. J. (2016). Effectiveness of a deep-sea cold-water coral marine protected area following eight years of fisheries closure. *Biological Conservation*, *200*, 60–69.

Johnson, C., Sherwin, T., Smythe-Wright, D., Shimmield, T., & Turrell, W. (2010). Wyville Thomson Ridge overflow water: Spatial and temporal distribution in the Rockall Trough. *Deep-Sea Research*, *57*, 1153–1162.

Kuijpers, A., Andersen, M. S., Kenyon, N. H., Kunzendorf, H., & van Weering, T. C. E. (1998). Quaternary sedimentation and Norwegian sea overflow pathways around Bill Bailey bank, north-eastern Atlantic. *Marine Geology*, *152*(1-3), 101–127.

Leith, C. E. (1996). Stochastic model of chaotic systems. *Physica D*, *98*, 481–491.

Mamaev, O. I. (2010). *Temperature-salinity Analysis of World Ocean Waters* (p. 373). Amsterdam: Elsevier.

Marshall, J., Adcroft, A., Hill, C., Perelman, L., & Heisey, C. (1997). A finite-volume, incompressible Navier-Stokes model for studies of the ocean on the parallel computers. *Journal of Geophysical Research*, *102*, 5733–5752.

Masson, D. G., Bett, B. J., Billet, D. S. M., Jacobs, C. L., Wheeler, A. J., & Wynn, R. B. (2003). The origin of deep-water, coral-topped mounds in the northern Rockall Trough, Northeast Atlantic. *Marine Geology*, *194*, 159–180.

McCurtney, M. S., & Mauritzen, C. (2001). On the origin of the warm inflow to the Nordic Seas. *Progress in Oceanography*, *51*, 125–214.

Pacanowski, R. C., & Philander, S. G. H. (1981). Parameterisation of vertical mixing in numerical models of tropical oceans. *Journal of Physical Oceanography*, *11*, 1443–1451.

Riemenschneider, U., & Legg, S. (2007). Regional simulations of the Faroe Bank Channel overflow in a level model. *Ocean Modelling*, *17*, 93–122.

Saunders, P. (1990). Cold outflow from the Faroe Bank Channel. *Journal of Physical Oceanography*, *20*, 29–43.

Sea-Bird Electronics (2011). Application note No.87: Calculaing calibration coefficients for WET labs ECO-BB scattering/turbidity meter (voltage or RS-232 output sensor) 3p.

Sherwin, T. J. (1991). Evidence of a deep internal tide in the Faroe Shetland Channel. In B. B. Parker (Ed.), *Tidal Hydrodinamics* (pp. 469–488). New York: John Wiley.

Sherwin, T. J. (2010). The observed 2D velocity structure of a fast and deep oceanic density current constrained in a gully. *Journal of Geophysical Research*, *115*, C03013. https://doi.org/10.1029/2009JC005557

Sherwin, T. J., Aleynik, D., Dumont, E., & Inall, M. E. (2015). Deep drivers of mesoscale circulation in the central of Rockall Trough. *Ocean Science*, *11*, 345–359.

Sherwin, T. J., Griffith, C. R., Inall, M. E., & Turrell, W. R. (2008). Quantifying the overflow across the Wyville Thomson Ridge in to the Rockall Rough. *Deep Sea Research*, *I*(55), 396–344.

Sherwin, T. J., & Turrell, W. R. (2005). Mixing and advection of a cold water cascade over the Wyville Thomson Ridge. *Deep Sea Research*, *I*(52), 1392–1413.

Stashchuk, N., Vlasenko, V., & Sherwin, T. J. (2010). Insights into the structure of the Wyville Thomson Ridge overflow current from a fine-scale numerical model. *Deep Sea Research*, *I*(57), 1192–1205.

Stashchuk, N., Vlasenko, V., & Sherwin, T. J. (2011). Numerical investigation of deep water circulation in the Faroese Channels. *Deep Sea Research*, *I*(58), 787–799.

Turrell, W. R., & Sherwin, T. J. (2003). A re-examination of the Wyville Thompson Ridge overflow, and its relevance to fluxes west of Britan. In *ICES Annual Science Conference* (CM 2003/T:08, pp. 1–18). Tallinn